Low Computational-cost Cell Detection Method for Calcium Imaging Data

Tsubasa Ito[a,b], Keisuke Ota[b], Kanako Ueno[b], Yasuhiro Oisi[b], Chie Matsubara[b], Kenta Kobayashi[c], Masanori Murayama[b], Toru Aonishi[d,b]

[a]*Interdisciplinary Graduate School of Science and Engineering, Tokyo Institute of Technology, Kanagawa, Japan*
[b]*RIKEN Center for Brain Science, Saitama, Japan*
[c]*Section of Viral Vector Development, National Institute for Physiological Sciences, Okazaki, Japan*
[d]*School of Computing, Tokyo Institute of Technology, Kanagawa, Japan*

Abstract

The rapid progress of calcium imaging has reached a point where the activity of tens of thousands of cells can be recorded simultaneously. However, the huge amount of data in such records makes manual analysis difficult. Consequently, there is a pressing need for automatic analysis for large-scale image data. Some automatic cell detection methods use machine learning, but their scalability to the data size remains a fundamental problem; they cannot be completed within a practical period of time on large-scale data acquired with recently developed ultra-large field-of-view microscopies. Here, we propose a low computational-cost cell detection (LCCD) method, which can process huge amounts of data within a practical period. We compared it with two previously proposed methods, constrained non-negative matrix factorization and Suite2P. The detection accuracy of LCCD was close to those of the other methods, whereas its calculation time was about ten times shorter.

Keywords: automatic cell detection, filter-based approach, calcium imaging, ultra-large field-of-view microscope

1. Introduction

The activities of many nerve cells can now be measured simultaneously for a long time, and with this capability, long-term temporal changes in the information representation of a neuronal population and functional interaction

within it can be investigated (Ziv et al., 2013). The rapid progress of imaging technology has made it possible to carry out such research. For example, various high-efficiency fluorescent calcium indicator proteins have been developed, including GCaMP which has high fluorescence intensity (Chen et al., 2013). Regarding progress in imaging devices, a miniaturized microscope mounted on the head of a mouse has enabled long-term measurements of neural population activities during long-term behaviors and learning (Ziv et al., 2013). Furthermore, several number of research groups have developed very wide field-of-view two-photon microscopies capable of imaging areas of square millimeter order (Stirman et al., 2016; Sofroniew et al., 2016). Such ultra-large field-of-view microscopies have made it possible to image the activities of several thousand to several tens of thousands of cells at single-cell resolution.

The first step of an analysis of multi-cellular image data is identification of the positions of the individual cells as regions of interest (ROIs) within the image; this step is called 'cell detection' (Lutcke and Helmchen, 2011). Manual identification of ROIs is effective, but it needs a lot of time and effort. As the data size becomes larger, manual cell detection is becoming more and more difficult, and demand for automate cell detection is increasing. Here, several number of automatic cell detection methods using machine learning have come to be used. Mukamel et al. (2009) proposed a cell detection method using the principal component analysis (PCA)-independent component analysis (ICA) algorithm. Moreover, several methods using non-negative matrix factorization (NMF) have been proposed. In particular, Maruyama et al. (2014) proposed background-constrained NMF (BC-NMF), which contains a background fluorescence model; it was shown to outperform the PCA-ICA method in noisy situations. Pnevmatikakis et al. (2016) proposed a constrained NMF (CNMF) with an autoregressive model for describing transient changes in neural calcium profiles. CNMF was shown to outperform both PCA-ICA and BC-NMF. Marius et al. (2016) proposed a NMF based method called Sute2P, which contains a model of background fluorescence changes due to neuropil activities. Different from these NMF methods, Reynolds et al. (2017) proposed ABEL, a method based on an active contour model. It has been reported that ABEL outperforms CNMF and is comparable in performance to Suite2P.

Since all the above methods are formulated as cost-function optimizations, they are very costly in terms of their computation and memory requirements when dealing with large-scale image data. In addition, the number of cells

able to be measured at single-cell resolution is rapidly increasing thanks to rapid progress in imaging technology. As demonstrated in this paper, it is difficult for such optimization-based methods to process large-scale image data acquired with the latest ultra-large field-of-view microscopies within a practical period of time at the current limits of computing power. For this reason, we developed a low computational-cost cell detection (LCCD) method adaptable to large-scale image data acquired with the latest ultra-large field-of-view microscopies. We confirmed with real data and artificial data that LCCD performed comparably to CNMF and Suite2P, whereas its calculation time was ten times shorter than those of the CNMF and Suite2P. In particular, LCCD could complete a cell detection task using artificial data mimicking data on the scale of ultra-large field-of-view microscopies in a reasonable amount of time, whereas CNMF and Suite2P could not do so. In addition, we developed a graphic user interface (GUI) to manually correct ROIs automatically assigned to detected cells and a module to correct for neuropil contamination by subtracting the neuropil signal from the cell signal.

2. Materials and Methods

2.1. Outline of LCCD

Figure 1 shows the outline of the LCCD procedure.

First, to remove slow temporal trends and shot noise from the image data, pixels that have been temporally smoothed by a long moving average filter with a width of 100 frames are subtracted from corresponding pixels temporally smoothed by a short moving average filter with a width of several frames. Then all the negative values of the denoised trend-subtracted data are forced to zero (Fig. 1(A)).

Next, the maximum luminance value at each pixel of the denoised trend-subtracted data is used to make a maximum luminance variation map (Fig. 1(B)).

An on-center off-surround filter and positive half-wave rectification are then applied to the maximum luminance variation map to emphasize the elliptical shape of cell bodies and reduce the background luminance including neuropil signals. The on-center off-surround filter is constructed by subtracting a two-dimensional averaging filter (11×11 pixels) from a two-dimensional Gaussian filter (std = 2.5 pixels). The filter size and standard deviation of the Gaussian are manually adjusted according to the expected cell body size (Fig.1(C)).

The contrast of the filtered map is emphasized with contrast-limited adaptive histogram equalization (Zuiderveld, 1994). As a result, the difference in luminance between the background and cells is made uniform throughout the map (Fig.1(D)).

After that, the contrast-emphasized map is binarized with a threshold value determined by the Otsu method (Otsu, 1979), and closed regions are detected with an eight-connected-component labeling operation. Next, only the closed regions having areas ranging from 20 to 300 pixels are picked up, and elongated ROIs are excluded with an oval filter. The oval filter can be easily realized by measuring the following two geometric characteristics of closed regions with the regionprops function in the MATLAB Image toolbox. One characteristic is the eccentricity of the ellipse that has the same second moments as a closed region. The other is the area ratio between a closed region and an ellipse having the same normalized second central moments as the region. Here, we selected closed regions only satisfying conditions that the eccentricity is less than 0.99 and the area ratio is less than 1.8. By applying the oval filter to the detected closed regions, somata are identified as oval-shaped ROIs (Fig. 1(E)).

If a few different cells are set as a single ROI, the merged ROI can be divided into individual cell ROIs manually by using a graphical user interface (GUI) (Fig. 1(F)). Conversely, if a single cell is separated into several ROIs, the separated ROIs can be manually combined into one with the GUI.

2.2. Compared cell detection methods

CNMF is an NMF-based method that incorporates an autoregressive model of calcium transient dynamics as a temporal constraint. In the program package, the user can choose one of two methods, greedy or sparse, as preprocessing to roughly detect cells. In this study, we chose greedy, which is recommended to be used for detecting cell bodies in the same situation as this research. The CNMF program package used for comparison was downloaded from `https://github.com/epnev/ca_source_extraction` (Pnevmatikakis et al., 2016). In the numerical experiments, the parameters of the CNMF (the std of the gaussial kernel, number of components to be found, order of autoregressive system, etc.) were manually set to maximize the performance of its cell detection. For a fair comparison with other methods with reference to manually identified somata ROIs, we only picked up closed regions having an area of 20 to 300 pixels, and we excluded elongated ROIs with the oval filter used by LCCD.

Suite2P is an NMF method that incorporates a model of background fluorescence changes due to neuropil activities. It has been reported that Suite2P outperforms CNMF. The Suite2P program package used for comparison was downloaded from `https://github.com/cortex-lab/Suite2P` (Marius et al., 2016). In the numerical experiments, the parameters of Suite2P (ops0.nSVDforROI, ops0.NavgFramesSVD, ops0.diameter, etc.) were manually set so as to maximize its performance.

The numerical experiments did not involve any manual editing of ROIs determined by the various cell detections so that only their abilities would be compared.

2.3. Two-photon calcium imaging data

We performed two-photon calcium imaging of L2/3 cortical neurons in an awake mouse. The images (512 $\times$ 512 pixels, 800μm $\times$ 800 μm) were acquired at 7.5 Hz using a custom-modified multiphoton microscope (Nikon, A1MP multiphoton confocal). The objective was a 16$\times$ water immersion lens (Nikon, 0.8 NA), and the light source was a femtosecond pulsed laser (Spectra-Physics, Mai Tai DeepSee) tuned to 920 nm. The imaging depth was ˜135 μm below the pia. The calcium sensor was GCaMP6f (Chen et al., 2013) which was expressed using an adeno-associated virus (AAV) vector.

2.4. Computational environment

All programs of LCCD, CNMF, and Suite2P were implemented in MATLAB (MathWorks). The computer used in the numerical experiments had four 22-core Intel (R) Xeon (R) E-7-8880 V4@ 2.2GHz processors (total of 88 cores/176 threads) with a total of 2TB RAM (HPCTECH). The operating system was a Cent-OS 6.7.

2.5. Synthesized artificial data

To evaluate the scalability of the methods, we synthesized artificial movies mimicking large-scale calcium-imaging data. We generated three movies with the following scales: 225 cells in 256 $\times$ 256 pixels, 841 cells in 512 $\times$ 512 pixels, 3136 cells in 1024 $\times$ 1024 pixels and 10000 cells in 2048 $\times$ 2048 pixels. Each of the four movies consisted of 5000 frames.

Each cell with an oval shape was placed on a point slightly randomly shifted from a two-dimensional lattice, and its orientation was randomly determined. Calcium transients in each cell were mimicked by an exponential decay function with a time constant of 5 frames, and its initializing time

point obeyed a simple Bernoulli process with a probability of initialization equal to 1.5 % per frame. For simplicity, the time constant of the exponential decay functions, the maximum rising amplitudes and frequencies of transients were assumed to be uniform in all cells and all frames. Static background fluorescence mimicked by a two-dimensional Gaussian function was added to these cells' signals. Here, the maximum rising amplitude of each transient and the maximum background fluorescence were each kept constant at 1000. Lastly, the artificial movies were synthesized through a shot noise process obeying a Poisson distribution whose intensity parameter was set to be the signal amplitude of each pixel.

2.6. Statistical Measures in the Performance Evaluation

ROIs were manually placed at individual cells detected with the naked eye. These manually obtained ROIs (see Fig. 2) were used as the ground truth (GT) in the performance evaluations. We quantified the level of matching between the GT ROIs and the automatically obtained ROIs by using the following statistical measures.

First, cross-correlation coefficients between all possible pairs of GT ROIs and automatically obtained ROIs were calculated, and all such pairs were sorted in descending order of cross-correlation coefficient. Next, the most matched pair of a GT ROI and an automatically obtained ROI was selected; then, the next most matched pair, which was not the previously selected ROI pair, was selected. This selection procedure was repeated until there were no pairs with non-zero correlation.

If an automatically obtained ROI was correlated with its pair GT ROI with a correlation coefficient of more than 0.6, it was counted as a true positive TP. If it did not meet these conditions, it was counted as a false positive FP. A GT ROI not paired with any TP automatically obtained ROI was counted as a false negative (FN).

Under the above definitions of TP, FP, and FN, the precision, recall, and success rate were calculated as performance measures. Precision was defined as the proportion of true positives among the total number of automatically obtained ROIs, i.e. $Precision = TP/(TP + FP)$, while recall was defined as the proportion of the number of GT ROIs paired TP ROIs among the total number of GT ROIs, i.e. $Recall = TP/(TP + FN)$. The success rate was defined as the harmonic mean between $Precision$ and $Recall$.

3. Results

3.1. Results of LCCD

To evaluate the performance of LCCD, we used it to detect somata from in vivo-calcium imaging data of a mouse cerebral neocortical 2/3 layer. Figure 2 shows ROIs drawn on 808 cells detected using LCCD. Note that in this experiment, we did not use the GUI to manually edit the automatically obtained ROIs. The details of the image data used here are described in the Materials and Methods. The parameters of LCCD, i.e., the length of the moving average filters, the size of the on-center off-surround filters and so on, were manually tuned so that LCCD could detect as many separated cells as possible. The values of those parameters are described in the Materials and Methods. It has been pointed out that elongated ROIs could be classified into parts of neurites including dendrites (Helmchen et al., 2001). In this study, we excluded elongated ROIs by using the oval filter described in the Materials and Methods.

Figure 2(B) shows a histogram of areas of the 808 ROIs obtained using LCCD. The area of each ROI can be estimated by counting its pixel number. 90% of the ROIs have an area less than $200\mu m^2$, which corresponds to the speculated size of a single somata under the experimental conditions. Thus, we presumed that almost all of the ROIs can be classified into somata, while individual ROIs of more than $200\mu m^2$ may capture a few different somata.

Figure 2(C) shows closeup views of representative ROIs and their calcium activities. Here, the neuropil signals were cancelled from the fluorescence time series by using the following method. The temporal profiles of the calcium activities show rapid calcium transients.

It has been reported that out-of-focus fluorescence from neuropil surrounding cells may contaminate fluorescence time series of cells (Dombeck et al., 2007). Recently, several research groups have sought to cancel contaminating neuropil signals from cell fluorescence signals (Keemink et al., 2018). The program package we developed allows the neuropil signal to be canceled out. Figure 2(D) shows the cancelation method implemented in it. In Fig. 2(D)(1), F^{in} is the original fluorescence time series of a single ROI. In Fig. 2(D)(2), f^{out} is a fluorescence time series of a wide region excluding ROIs. f^{out} is calculated by applying a two-dimensional spatial Gaussian filter to the image data masked by the ROIs, i.e. the image data forced to zero within the ROIs. Here, the standard deviation of the Gaussian filter was set to 20 pixels ($30\mu m$), which was the same order of distance as used in

(Chen et al., 2013). The corrected calcium activity of a single cell shown in Fig. 2(D)(3) was obtained by subtracting αf^{out} from F^{in}. The coefficient α is the amplitude in the f^{out} subtraction, which was determined heuristically (Chen et al., 2013); we used $\alpha = 0.8$. Comparing F^{in} with the corrected signal in Fig. 2(D)(3), it can be seen that the slow component of F^{in} has been removed and the calcium transients are clear.

3.2. Comparison of LCCD with CNMF and Suite2P

We compared the performances of LCCD, CNMF (Pnevmatikakis et al., 2016) and Suite2P (Marius et al., 2016) on the data shown in Fig. 2. We used the distribution codes of CNMF and Suite2P available from Github (see the Materials and Methods). To compare their cell detection abilities by themselves, we did not carry out manual editing of the ROIs they obtained.

Figure 3 shows ground truth (GT) ROIs (i.e. manually detected ROIs by researchers) and ROIs automatically obtained with LCCD, CNMF, and Suite2P. The number of GT ROIs was 794. The numbers of ROIs obtained using LCCD, CNMF, and Suite2P were 808, 785, and 943, respectively. The sizes of the LCCD ROIs are similar to those of the GT ROIs, whereas the sizes of the CNMF and Suite2P ROIs are larger than those of the GT ROIs. Note that the CNMF and Suite2P parameters that were related to the size of the ROIs were manually tuned so that the performance of each method was maximized. Furthermore, as shown in Fig. 3, the CNMF ROIs were strongly localized in brighter image regions where the level of GCaMP expression was high, whereas the LCCD and Suite2P ROIs were comparably distributed over brighter as well as darker image regions.

To compare the performance of LCCD with those of CNMF and Suite2P statistically with reference to the GT, we calculated the precision, recall, and success rate (see the Materials and Methods). As shown in Table 1, the recall of Suite2P was 63.4%, which was prominently the highest among the three methods, but its precision was 51.3%, the lowest among the three methods. This means that Suite2P detected the most TP ROIs, but it also detected the most FP ROIs. The success rate (i.e. the harmonic mean between recall and precision) of Suite2P was 56.7%, which was highest among the three methods. In contrast, the precision of LCCD was 52.6%, which was highest among the three methods, and its recall was 55.6%, which was intermediate among the three methods. This means that LCCD detected the least FN ROIs, while it detected an intermediate number of TP ROIs. The success rate of LCCD was 54.1%, which was intermediate among the three methods.

On the other hand, the recall of CNMF was the lowest, and its precision was almost the same as the lowest value of Suite2P. Thus, the success rate of CNMF was lowest among the three methods.

Next, we compared the scalability of LCCD with those of CNMF and Suite2P. In a numerical experiment, we measured the calculation time of the three methods running on the same high-performance computer and processing four synthesized imaging data: 225 cells in 256 × 256 pixels, 841 cells in 512 × 512 pixels, 3136 cells in 1024 × 1024 pixels and 10000 cells in 2048 × 2048 pixels (see the Materials and Methods). Each line of Fig. 4, indicates the calculation time of each method as a function of synthesized data size. No line means that the process hung up or could not be completed after several days. As shown in Fig. 4, Suite2P did not complete its process on 1024 × 1024 and 2048 × 2048 pixels of data, and the CNMF did not complete its process on 2048 × 2048 pixels of data. On the other hand, LCCD completed its process on all four datasets, and its calculation was over ten times shorter than those of the other methods. For instance, LCCD took 9 minutes to process 1024 × 1024 pixels of data, whereas CNMF took 140 minutes. Furthermore, LCCD took 24 minutes to process 2048 × 2048 pixels of data, whereas the other methods had not completed the cell detection process after several days.

3.3. Graphic user interface

We developed a GUI with which users can manually edit ROIs obtained with LCCD (Fig. 5). If users find a few different cells have been merged into a single ROI, they can manually divide the merged ROI into individual cell ROIs. Furthermore, if they find a single cell that has been separated into several ROIs, they can manually combine the separated ROIs into one.

4. Discussion

4.1. Summary of Results and Conclusion

We developed a low computational-cost cell detection method that can operate on large-scale image data that are acquired with ultra-large field-of-view microscopies. We confirmed with real in-vivo data and synthesized data that its detection ability is comparable to that of CNMF and Suite2P, whereas its calculation time is over ten times shorter when each method is run on the same high-performance computer. In an experiment, LCCD completed its entire process within a reasonable amount of time on 2048 ×

2048 synthesized data that mimicked large-scale data obtained with the latest ultra-large field-of-view microscopy (Stirman et al., 2016), while CNMF and Suite2P could not complete their processes on the same data. Consequently, we believe that LCCD will make it possible to detect cells from large-scale data obtained with ultra-large field-of-view microscopy within a practical time and with an accuracy comparable to that of state-of-art methods such as CNMF and Suite2P. In addition, we developed a GUI to manually correct ROIs assigned to automatically detected cells and a module to correct for neuropil contamination by subtracting the neuropil signal from the cell signal. In the future, we will extend the functional modules of our program package in accordance with user requests.

4.2. Why does LCCD have an accuracy comparable to state-of-art methods?

LCCD is a simple filter-based method. We will point out two key factors why it is comparable in accuracy to Suite2P.

One factor is the use of an on-center off-surround filter and positive half-wave rectification (Fig. 1 (C)). The on-center off-surround filter is a kind of band pass filter. Thus, by tuning the filter size and standard deviation of the Gaussian according to the expected cell body size, this filter can emphasize the elliptical shape of cell bodies and reduce the background luminance including neuropil signals (Fig. 2 (D)). Chen et al. (2013) pointed out that out-of-focus fluorescence from surrounding neuropil cells can contaminate fluorescence time series of cells and the contaminated neuropil signal can disturb automatic cell detections, because it induces strong correlations between the cells' signal and the background signal. To overcome this problem, Suite2P seeks to cancel out the contaminated neuropil signal by incorporating a model of neuropil activities. On the other hand, LCCD cancels the neuropil signal by using the on-center off-surround filter and positive half-wave rectification.

The other factor is the use of contrast-limited adaptive histogram equalization. As shown in Fig. 3, the ROIs found by LCCD are distributed not only in brighter image regions but also in darker image regions. The spatial uniformity of ROIs obtained with LCCD is comparable to that of Suite2P. This uniformity is achieved by the contrast-limited adaptive histogram equalization. By applying this algorithm, the difference in luminance between the background and the cells is made uniform throughout the map (Fig. 1(D)), Thus, we can detect cells not only from brighter image regions but also from darker image regions by using a simple thresholding method.

4.3. Weak point of LCCD and improvement method

Most serious weak point of LCCD is that it cannot in principle separate overlapping cells into individual cells because it does not fully utilize temporal information. LCCD achieves high-speed cell detection at the sacrifice of temporal information. Two-photon excitation microscopies have a very narrow focal region resulting in a high resolution in the z-direction. In taking an image with two-photon microscopies, it is unlikely that cells overlap within the focal region. Thus, as demonstrated in this paper, LCCD works very well in practical situations.

However, there are cases that cells are very close in the two-dimensional focal plane partially overlap. To improve the ability of LCCD in this regard, we need to take the following temporal division approach. First, divide up the data into several short time frames. Next, use LCCD to detect cells as ROIs from each of the divided data. Finally, integrate these ROIs by using the clue of spatial overlap between temporally different ROIs. In the next report, we will focus on this temporal division version of LCCD, called extended LCCD (exLCCD).

Acknowledgements

This study was supported by the Cooperative Study Program of the National Institute for Physiological Sciences. The authors are grateful for support from the Japan Society for Promotion of Science, KAKENHI JP16H01539 and JP16H01269 to T.A. This research was partially supported by the program for Brain Mapping by Integrated Neurotechnologies for Disease Studies (Brain/MINDS) from the Japan Agency for Medical Research and Development, AMED under the Grant Number JP18dm0207001h0005. This research was also supported by a CREST grant (Grant Number JPMJCR1861) from the Japan Science and Technology Agency.

References

Chen, T.W., Wardill, T.J., Sun, Y., Pulver, S.R., Renninger, S.L., Baohan, A., Schreiter, E.R., Kerr, R.A., Orger, M.B., Jayaraman, V., Looger, L.L., Svoboda, K., Kim, D.S., 2013. Ultrasensitive fluorescent proteins for imaging neuronal activity. Nature 499, 295–300. URL: `http://www.ncbi.nlm.nih.gov/pubmed/23868258`, doi:`10.1038/nature12354`.

Dombeck, D.A., Khabbaz, A.N., Collman, F., Adelman, T.L., Tank, D.W., 2007. Imaging large-scale neural activity with cellular resolution in awake, mobile mice. Neuron 56, 43–57.

Helmchen, F., Fee, M.S., Tank, D.W., Denk, W., 2001. A miniature head-mounted two-photon microscope: high-resolution brain imaging in freely moving animals. Neuron 31, 903–912.

Keemink, S.W., Lowe, S.C., Pakan, J.M., Dylda, E., van Rossum, M.C., Rochefort, N.L., 2018. Fissa: A neuropil decontamination toolbox for calcium imaging signals. Scientific reports 8, 3493.

Lutcke, H., Helmchen, F., 2011. Two-photon imaging and analysis of neural network dynamics. Reports on Progress in Physics 74, 086602.

Marius, P., Carsen, S., Mario, D., Sylvia, S., L. Federico, R., Henry, D., Matteo, C., Kenneth, D.H., 2016. Suite2p: beyond 10,000 neurons with standard two-photon microscopy. doi:10.1101/061507.

Maruyama, R., Maeda, K., Moroda, H., Kato, I., Inoue, M., Miyakawa, H., Aonishi, T., 2014. Detecting cells using non-negative matrix factorization on calcium imaging data. Neural Netw 55, 11–9. URL: http://www.ncbi.nlm.nih.gov/pubmed/24705544, doi:10.1016/j.neunet.2014.03.007.

Mukamel, E.A., Nimmerjahn, A., Schnitzer, M.J., 2009. Automated analysis of cellular signals from large-scale calcium imaging data. Neuron 63, 747–60. URL: http://www.ncbi.nlm.nih.gov/pubmed/19778505, doi:10.1016/j.neuron.2009.08.009.

Otsu, N., 1979. Threshold selection method from gray-level histograms. Ieee Transactions on Systems Man and Cybernetics 9, 62–66. URL: <GotoISI>://WOS:A1979GE96000010, doi:Doi10.1109/Tsmc.1979.4310076.

Pnevmatikakis, E.A., Soudry, D., Gao, Y., Machado, T.A., Merel, J., Pfau, D., Reardon, T., Mu, Y., Lacefield, C., Yang, W., Ahrens, M., Bruno, R., Jessell, T.M., Peterka, D.S., Yuste, R., Paninski, L., 2016. Simultaneous denoising, deconvolution, and demixing of calcium imaging data. Neuron 89, 285–99. URL: http://www.ncbi.nlm.nih.gov/pubmed/26774160, doi:10.1016/j.neuron.2015.11.037.

Reynolds, S., Abrahamsson, T., Schuck, R., Sjostrom, P.J., Schultz, S.R., Dragotti, P.L., 2017. Able: An activity-based level set segmentation algorithm for two-photon calcium imaging data. eNeuro 4. URL: http://www.ncbi.nlm.nih.gov/pubmed/29085906, doi:10.1523/ENEURO.0012-17.2017.

Sofroniew, N.J., Flickinger, D., King, J., Svoboda, K., 2016. A large field of view two-photon mesoscope with subcellular resolution for in vivo imaging. Elife 5. URL: <GotoISI>://WOS:000380909900001, doi:ARTNe1447210.7554/eLife.14472.

Stirman, J.N., Smith, I.T., Kudenov, M.W., Smith, S.L., 2016. Wide field-of-view, multi-region, two-photon imaging of neuronal activity in the mammalian brain. Nature Biotechnology 34, 857–+. URL: <GotoISI>://WOS:000381339600023, doi:10.1038/nbt.3594.

Ziv, Y., Burns, L.D., Cocker, E.D., Hamel, E.O., Ghosh, K.K., Kitch, L.J., El Gamal, A., Schnitzer, M.J., 2013. Long-term dynamics of ca1 hippocampal place codes. Nature Neuroscience 16, 264–266. URL: <GotoISI>://WOS:000315474800006, doi:10.1038/nn.3329.

Zuiderveld, K., 1994. Contrast limited adaptive histograph equalizationl. Gems IV Graphics .

Table 1: Statistical comparison of LCCD with CNMF and Suite2P with reference to ground truth. Precision, recall and success rate are indicated in the table.

Method	Success rate(%)	Recall(%)	Precision(%)
LCCD	54.1	55.6	52.6
CNMF	52.3	53.0	51.6
Suite2P	56.7	63.4	51.3

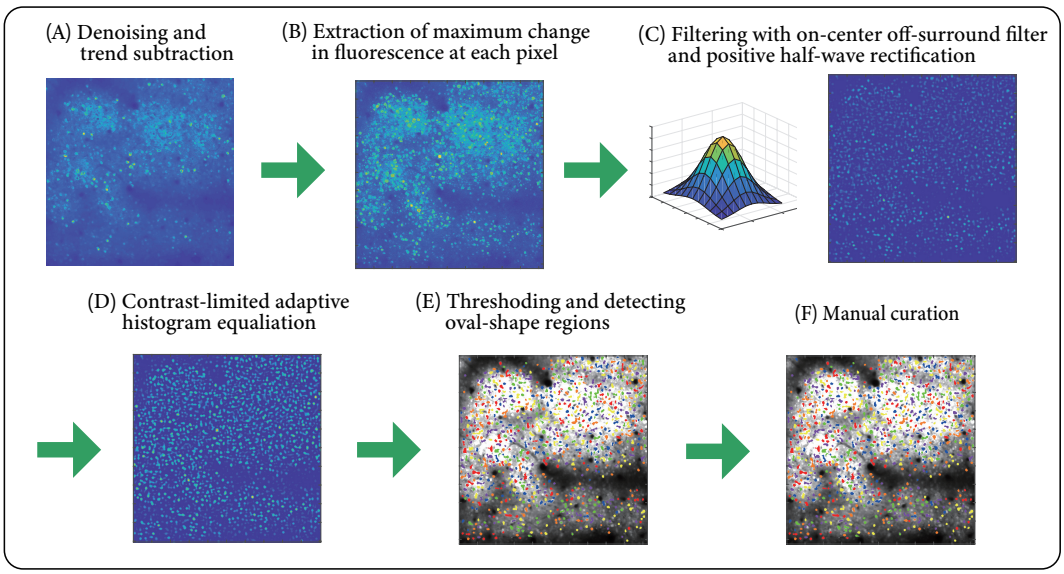

Figure 1: Overview of low computational-cost cell detection (LCCD) method. (A) At each pixel, image data temporally smoothed by a long moving average filter with a width of 100 frames is subtracted from image data temporally smoothed by a short moving average filter with a width of several frames. Then, all negative values of the denoised trend-subtracted data are forced to zero. (B) The maximum luminance value among all frames of the denoised trend-subtracted data is picked up at each pixel, and a maximum luminance variation map is created. (C) An on-center off-surround filter and positive half-wave rectification are applied to the maximum luminance variation map so as to emphasize the elliptical shape of cell bodies and reduce the background luminance including neuropil signals. (D) The contrast of the filtered map is emphasized with contrast-limited adaptive histogram equalization to make uniform differences between the background and cell luminance values throughout the map. (E) The contrast-emphasized map is binarized with a threshold value determined by the Otsu method, and closed regions are detected with the eight connected-component labeling operation. Then, by applying the oval filter, somata are identified as oval-shaped ROIs. (F) Users can select whether or not to manually edit the obtained ROIs.

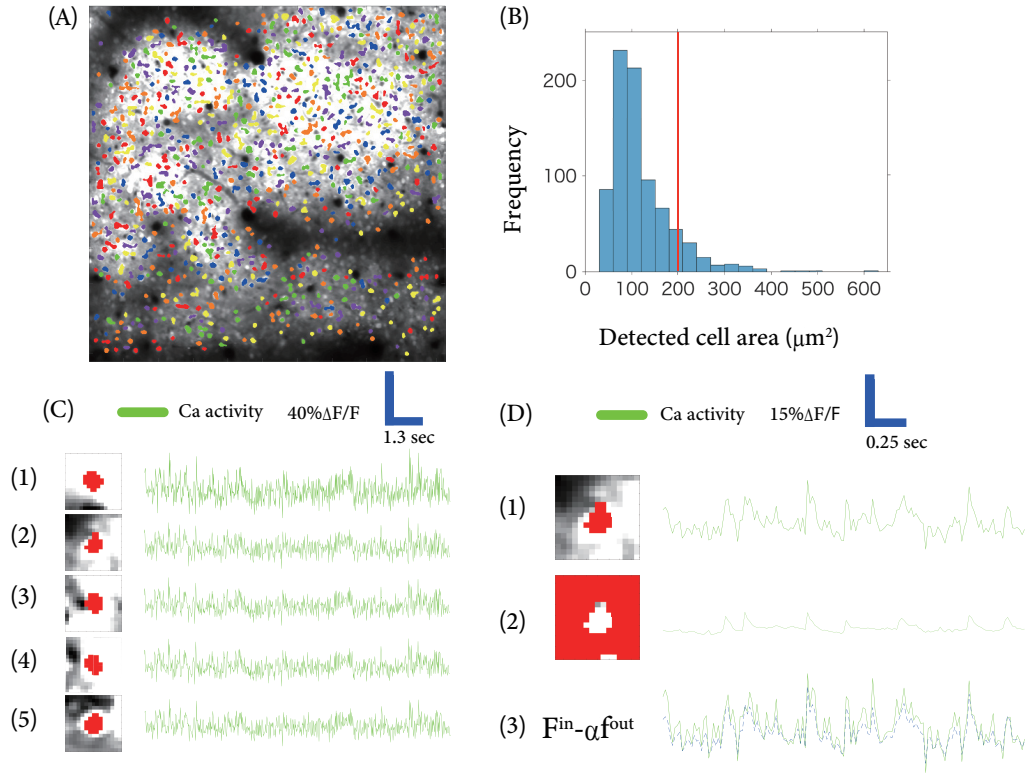

Figure 2: Results of applying LCCD to in vivo calcium-imaging data of a mouse cerebral neocortical 2/3 layer. (A) ROIs obtained using LCCD. 808 cells are detected. (B) Histogram of areas of the 808 ROIs. (C) Examples of ROIs and their calcium activities. Here, the neuropil signals have been cancelled from the fluorescence time series by using the standard method described in (D). (D) Neuropil signal cancelation method. (1) F^{in}: Original fluorescence time series of a single ROI. (2) f^{out}: Fluorescence time series of wide region excluding ROIs. f^{out} is calculated by applying a two-dimensional spatial Gaussian filter to the image data masked by the ROIs, i.e. by zero forcing within the ROIs. (3) Calcium activities of a single ROI corrected by subtracting αf^{out} from F^{in} (green solid line). Here, $\alpha = 0.8$. For comparison, we have superimposed F^{in} on this graph (blue dashed line).

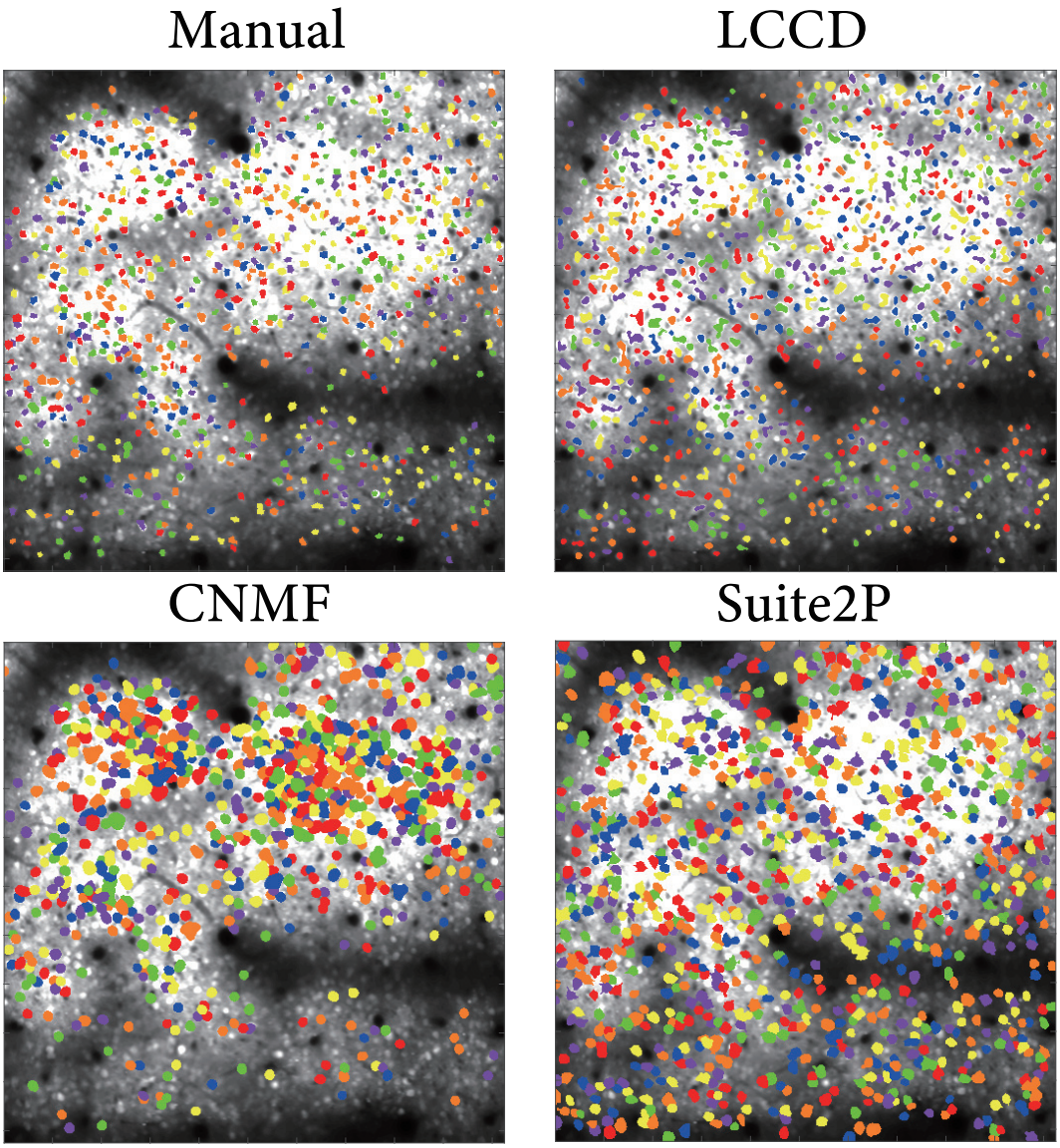

Figure 3: Ground-truth ROIs and ROIs automatically obtained with LCCD, CNMF, and Suite2P. (A) Ground-truth ROIs manually drawn on somata identified by researchers. ROIs obtained using LCCD (B), CNMF (C) and Suite2P (D). In each panel, the temporal average of the image data is shown as a gray-scale image, and ROIs are indicated as colored spots. The number of ground-truth ROIs is 794. The ROIs obtained using LCCD, CNMF, and Suite2P numbered 808, 785, and 943, respectively.

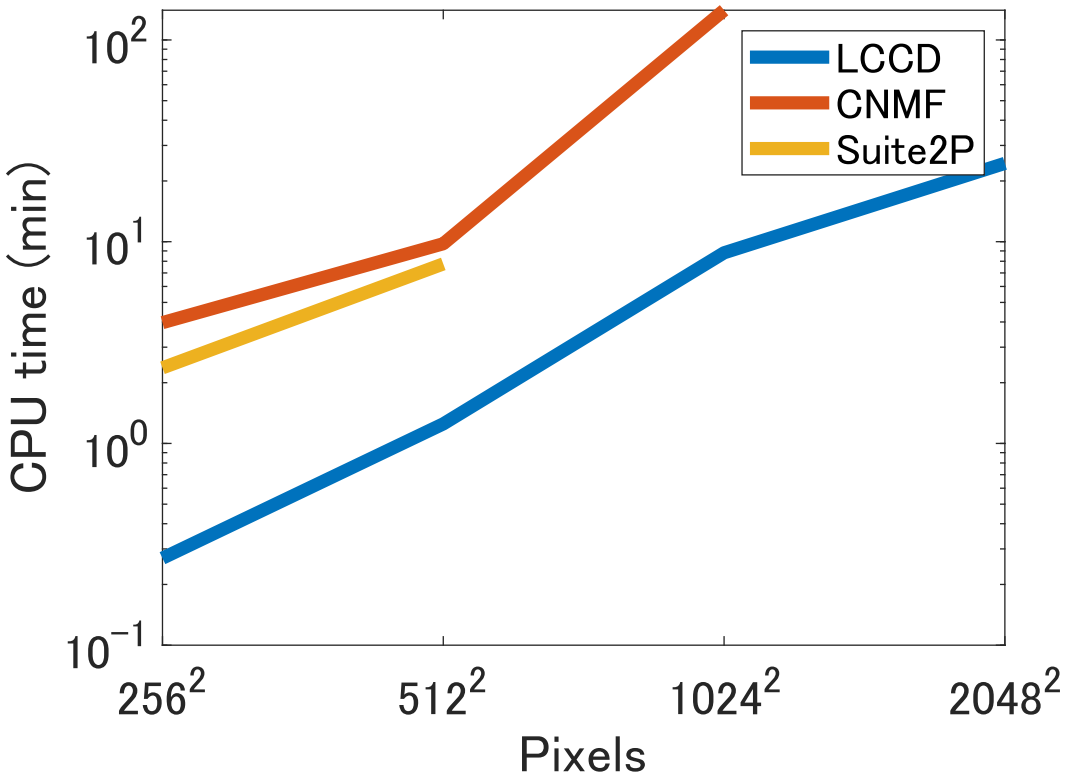

Figure 4: Comparison of scalability of LCCD, CNMF and Suite2P. Each line indicates the calculation time of each method as a function of the size of synthesized imaging data: 225 cells in 256 × 256 pixels, 841 cells in 512 × 512 pixels, 3136 cells in 1024 × 1024 pixels, and 10000 cells in 2048 × 2048 pixels. Each of the four data consist of 5000 frames. No line means that the process hung up or was not completed even after several days on a high-performance computer.

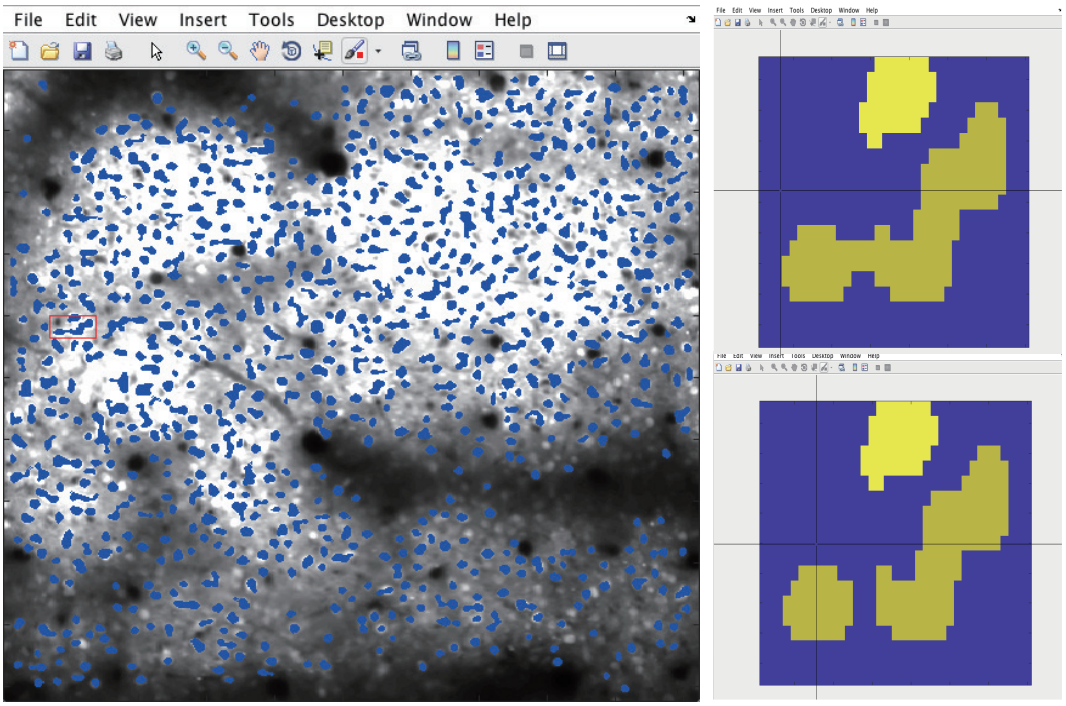

Figure 5: Graphical User Interface (GUI) for manual editing of ROIs obtained with LCCD. If a few different cells are set as a single ROI, the merged ROI can be divided into the ROIs of individual cells manually. If a single cell is separated into several ROIs, the separated ROIs can be manually combined into one.